

Quasi-nodal lines in rhombohedral magnetic materials

Rafael González-Hernández,^{1,2,*} Erick Tuiran,^{1,†} and Bernardo Uribe^{3,4,‡}

¹*Departamento de Física y Geociencias, Universidad del Norte,*

Km. 5 Vía Antigua Puerto Colombia, Barranquilla 080020, Colombia

²*Institut für Physik, Johannes Gutenberg Universität Mainz, D-55099 Mainz, Germany*

³*Departamento de Matemáticas y Estadística, Universidad del Norte,*

Km. 5 Vía Antigua Puerto Colombia, Barranquilla 080020, Colombia

⁴*Max Planck Institut für Mathematik, Vivatsgasse 7, 53115 Bonn, Germany*

(Dated: July 26, 2021)

A well-established result in condensed matter physics states that materials crystallizing in symmetry groups containing glide reflection symmetries possess nodal lines on the energy bands. These nodal lines are topologically protected and appear on the fixed planes of the reflection in reciprocal space. In the presence of inversion symmetry, the energy bands are degenerate and the nodal lines on the fixed plane may hybridize or may cross. In the former case, the crossing is avoided, thus producing lines on reciprocal space where the energy gap is small, and in the latter, the nodal lines will endure, thus producing Dirac or double nodal lines. In addition, if the material crystallizes in a ferromagnetic phase where the glide reflection symmetry is broken, the nodal lines hybridize, thus defining lines in reciprocal space where the energy gap is small. In this work we concentrate our efforts on the study of nodal lines that hybridize due to magnetization; we have coined the term of quasi-nodal lines for those lines in reciprocal space where the energy gap is small (less than what can be detected experimentally). We study magnetic trifluorides and trioxides which crystallize in magnetic space groups 167.107 and 161.71 and we show the existence of quasi-nodal lines on these materials. We furthermore show that whenever the quasi-nodal lines are located around the Fermi level then interesting charge and spin transport effects are induced and can be used to detect experimentally these lines. Of particular interest are the half-metallic ferromagnetic phases of PdF_3 and LiCuF_3 where the large signal of the anomalous Hall conductance is due to the presence of the quasi-nodal lines on the Fermi level.

INTRODUCTION

Topological non-trivial states of matter have been investigated intensively in recent years in condensed matter physics and materials science [1–3]. The field has grown dramatically after the discovery of topological insulators and it is in continuous development with the prediction of diverse topological semimetals phases [4, 5]. Topological semimetals are materials with gapless bulk states and can be classified in Dirac, Weyl and nodal-line semimetals [6–8]. In contrast to Dirac and Weyl semimetals, which have zero-dimensional band crossings, nodal line semimetals have prolonged band crossings along unique lines in reciprocal space [9]. In particular, the nodal lines can cross the Brillouin zone in the shape of a closed line or a ring [10, 11]. These special band crossings can induce exotic phenomena and effects such as ultrahigh mobilities, extremely high conductivity, large magnetoresistance and unusual anomalous and spin Hall effects [12–18].

It has been found that the manifestation of nodal-lines in magnetic and nonmagnetic materials is directly related to the presence, absence or combination of symmetries as time-reversal, inversion, mirror, rotation and partial translation [19–23]. Depending on particular planes or lines in the reciprocal space that are protected by a set of these symmetries, nodal lines can also be categorized into Dirac and Weyl-type [24–26]. In Dirac nodal lines

both inversion symmetry and time-reversal symmetry should be present to guarantee a four degeneration along the band crossing [27–30]. On the other side, in Weyl nodal lines the lack of either time-reversal or inversion symmetry permits the band to split and the degeneracy is of degree two [24]. A recent discovery of protected Weyl nodal lines in ferromagnetic materials has attracted great attention because of their potential application in novel spintronic devices [31–35]. Hence, the study of crystalline symmetries that topologically predict nodal lines close to the Fermi level is one of the most important goals in this field.

On the other hand, it is well known that valence and conduction bands with the same symmetry eigenvalues can hybridize, leading to anticrossing points in band structures [36, 37]. However, depending of the system symmetries, these anticrossing points can be extended along the Brillouin zone showing a pattern similar to a nodal line; therefore they have been coined quasi-nodal line or nodal-line band anticrossings [38]. These quasi-nodal lines could also induce novel electronic and spin transport phenomena as it has been observed in nodal line semimetals [38, 39]. In this manuscript, We predict theoretically and detect computationally the formation of quasi-nodal lines in rhombohedral crystal structures, in particular, IrF_3 , LaAgO_3 , PdF_3 and LiCuF_3 , and we foresee that this study can be extended to a large set of magnetic and nonmagnetic rhombohedral materials

based on #161 and #167 space groups such as XF_3 , ABF_3 , XO_3 , ABO_3 and $\text{AB}(\text{PO}_4)_3$. In addition, using the linear response formalism [40, 41] we find that the quasi-nodal lines are responsible for a large signal of anomalous and spin Hall conductivity in these materials. It is expected that this novel topological transport behavior could lead to the design of novel spintronic devices.

NODAL AND QUASI-NODAL LINES ON GLIDE REFLECTION INVARIANT PLANES

Nodal lines appear on the fixed planes of glide reflection symmetries in reciprocal space [42]. They may hybridize or cross in the presence of inversion symmetry, and they hybridize in the ferromagnetic phases on which the glide reflection symmetry is broken. In this section we make a summary of the different types of nodal and quasi-nodal lines induced by glide reflection symmetries.

Nodal lines

Consider a system with spin-orbit coupling (SOC) which is invariant under a glide mirror reflection on a plane \mathcal{G} . We can write

$$\mathcal{G}(\mathbf{x}) = \sigma_{\mathbf{n}}(\mathbf{x}) + \mathbf{b}, \quad (1)$$

as the composition of the mirror reflection $\sigma_{\mathbf{n}}$ along the plane perpendicular to the unit normal vector \mathbf{n} and the partial translation by \mathbf{b} . Since \mathcal{G} is a glide reflection on the crystal, we have that \mathcal{G}^2 is a translation by the Bravais vector $\sigma_{\mathbf{n}}(\mathbf{b}) + \mathbf{b}$. Let us split the vector \mathbf{b} on its components parallel and perpendicular to \mathbf{n} :

$$\mathbf{b} = \mathbf{b}_{\mathbf{n}} + \mathbf{b}_{\mathbf{n}^\perp} \quad (2)$$

and note that $2\mathbf{b}_{\mathbf{n}^\perp} = \sigma_{\mathbf{n}}(\mathbf{b}) + \mathbf{b}$ and therefore $\mathbf{b}_{\mathbf{n}^\perp}$ is half a Bravais lattice vector. Hence we have in momentum coordinates

$$\mathcal{G}^2 = -e^{-i2\mathbf{k} \cdot \mathbf{b}_{\mathbf{n}^\perp}}. \quad (3)$$

Let us consider two consecutive energy bands and let us restrict them to the invariant planes of the operator \mathcal{G} . On these planes we have $\mathcal{G}(\mathbf{k}) = \sigma_{\mathbf{n}}(\mathbf{k}) = \mathbf{k}$. The band electron energies restricted to these planes are both 2-dimensional and therefore they intersect generically on a 1-dimensional manifold (the intersection might be empty). Whenever they intersect we obtain the so-called nodal lines. But how are these nodal lines protected?

Whenever the system preserves the time reversal symmetry \mathbb{T} we may focus our attention on the time reversal

invariant points in momentum space (TRIMs) located on the fixed plane by \mathcal{G} . Note that \mathcal{G} permutes the TRIMs, leaving always at least four fixed. The argument is the following. If all TRIMs are fixed by \mathcal{G} , then \mathbf{n} is one of the following three unit vectors:

$$(1, 0, 0), (0, 1, 0), (0, 0, 1) \quad (4)$$

Now, if Γ and Γ' are different TRIMs with $\Gamma' = \sigma_{\mathbf{n}}(\Gamma)$, then \mathbf{n} is parallel to $\Gamma - \Gamma'$. Checking the possibilities of $\sigma_{\mathbf{n}}(\pi, 0, 0)$ we see that the only possible unit vectors for \mathbf{n} are then the following:

$$\frac{1}{\sqrt{2}}(1, \pm 1, 0), \frac{1}{\sqrt{2}}(0, 1, \pm 1), \frac{1}{\sqrt{2}}(\pm 1, 0, 1) \quad (5)$$

Now, it is important to notice that the reflection $\sigma_{\mathbf{n}}$ fixes two disconnected planes in momentum space whenever \mathbf{n} is one of the vectors presented in (4), i.e. $k_l = 0$ and $k_l = \pi$ for $l \in \{x, y, z\}$, meanwhile it fixes only one connected plane whenever is one of the vectors presented in (5), i.e. $k_l \pm k_m = 0$ for $l \neq m$ and both in $\{x, y, z\}$.

The existence of a nodal line along the fixed plane by \mathcal{G} can be predicted if there are two different TRIMs Γ and Γ' along the plane with the property that their \mathcal{G} eigenvalues are different. If this is the case, the energy band diagrams of any path joining Γ and Γ' will produce an hourglass, and hence a band intersection along the path. Now since this argument works for any path between Γ and Γ' , then a nodal line must exist. The only requirement for this to happen is that $\mathbf{b}_{\mathbf{n}^\perp} \neq 0$, namely that the mirror reflection has a glide. If Γ is fixed by \mathcal{G} , then there must exist Γ' also fixed by \mathcal{G} such that $(\Gamma' - \Gamma) \cdot \mathbf{b}_{\mathbf{n}^\perp} \neq 0$ (this because \mathcal{G} fixes four TRIMs spanning the plane and $\mathbf{b}_{\mathbf{n}^\perp}$ belongs to the plane) and such that $(\Gamma' - \Gamma) \cdot 2\mathbf{b}_{\mathbf{n}^\perp} \equiv \pi \pmod{2\pi}$; this because $\mathbf{b}_{\mathbf{n}^\perp}$ is half Bravais vector and $2(\Gamma' - \Gamma)$ is a reciprocal lattice vector.

On Γ and Γ' the time reversal operator \mathbb{T} conjugates the eigenvalues of \mathcal{G} , and since the eigenvalues of \mathcal{G} differ by a sign, the only options for the eigenvalues of \mathcal{G} at Γ and Γ' are $\{1, -1\}$ and $\{i, -i\}$. Hence any path from Γ to Γ' on the fixed plane by \mathcal{G} induces an hourglass combinatorial diagram on the energy bands. The intersection of the middle bands is enforced because the eigenvalues of \mathcal{G} at that point differ by a sign, and therefore hybridization (or repulsion) is avoided [43]. A schematic diagram of the nodal line thus formed is presented in Fig. 1 (a).

Let us see some explicit examples:

a) Consider $\mathcal{G}(x, y, z) = (-x, y, z + \frac{1}{2})$ with $\mathbf{n} = (1, 0, 0)$ and $\mathbf{b} = \mathbf{b}_{\mathbf{n}^\perp} = (0, 0, \frac{1}{2})$. We have $\mathcal{G}^2 = -e^{ik_z}$ and the fixed planes are $k_x = 0$ and $k_x = \pi$. In both planes we get nodal lines that must intersect any path joining TRIMs with $k_z = 0$ to TRIMs with $k_z = \pi$; therefore these nodal lines should cross the fixed plane along the k_y -direction.

b) Note that the previous argument can be applied without any change to the operator $\mathcal{G}(x, y, z) = (-x + \frac{1}{2}, y, z + \frac{1}{2})$ where $\mathbf{b}_{\mathbf{n}} = (\frac{1}{2}, 0, 0)$ and $\mathbf{b}_{\mathbf{n}^\perp} = (0, 0, \frac{1}{2})$. The component of the translation along the direction of \mathbf{n}

plays no role on the existence of the nodal lines protected by the hourglasses. This symmetry appears in the space group #14 ($P2_1/c$).

c) Consider $\mathcal{G}(x, y, z) = (y + \frac{1}{2}, x + \frac{1}{2}, z + \frac{1}{2})$ with $\mathbf{n} = \frac{1}{\sqrt{2}}(1, -1, 0)$ and $\mathbf{b} = \mathbf{b}_{\mathbf{n}^\perp} = (\frac{1}{2}, \frac{1}{2}, \frac{1}{2})$. We have $\mathcal{G}^2 = -e^{-i(k_x+k_y+k_z)}$ and the fixed plane is $k_x = k_y$. The nodal lines must meet all paths joining TRIMs along $k_z = 0$ with TRIMs along $k_z = \pi$

Note that whenever the translation vector \mathbf{b} is parallel to the reflection vector \mathbf{n} , the \mathcal{G} eigenvalues are constant $\pm i$ along the fixed planes. Therefore if the energy bands with different eigenvalues intersect, then there cannot be hybridization and these nodal lines that appear are called *accidental*.

In the presence of the inversion symmetry, all the energy bands are degenerate by Kramer's rule. Some of the nodal lines previously described survive meanwhile in other cases the bands hybridize thus avoiding the nodal line. In the latter case, we get what is known as *anticrossings* and they are of interest whenever the energy band gap is small.

Double nodal lines

Let us now suppose that we have time reversal symmetry \mathbb{T} , inversion symmetry \mathcal{I} and the glide reflection \mathcal{G} as in Eqn. (1). In position coordinates we have

$$\mathcal{G}(\mathcal{I}(\mathbf{x})) = \mathcal{I}(\mathcal{G}(\mathbf{x})) + 2\mathbf{b}, \quad (6)$$

implying thus that \mathbf{b} is also half a Bravais lattice vector (hence we have that all three vectors \mathbf{b} , $\mathbf{b}_{\mathbf{n}}$ and $\mathbf{b}_{\mathbf{n}^\perp}$ are half Bravais vectors); therefore in momentum coordinates

$$e^{-i2\mathbf{k}\cdot\mathbf{b}}\mathcal{I}\mathcal{G} = \mathcal{G}\mathcal{I}. \quad (7)$$

The composition of the inversion with the time reversal operator $\mathbb{T}\mathcal{I}$ leaves momentum coordinates fixed and squares to -1 , thus endowing the energy eigenvalues of the Hamiltonian with a quaternionic structure. This implies that all energy states come in degenerate pairs due to Kramer's rule. Let us see what happens to the \mathcal{G} eigenvalues of a Kramer pair once restricted to the fixed planes of \mathcal{G} whose equations are

$$2\mathbf{n}(\mathbf{k}\cdot\mathbf{n}) \equiv 0 \pmod{\mathbf{G}} \quad (8)$$

with \mathbf{G} reciprocal lattice vectors.

From Eqn. (7) we obtain the commutation relation between \mathcal{G} and $\mathbb{T}\mathcal{I}$:

$$e^{-i2\mathbf{k}\cdot\mathbf{b}}(\mathbb{T}\mathcal{I})\mathcal{G} = \mathcal{G}(\mathbb{T}\mathcal{I}). \quad (9)$$

Now let us consider an eigenfunction of the Hamiltonian Ψ and let us restrict it to the fixed point planes of the

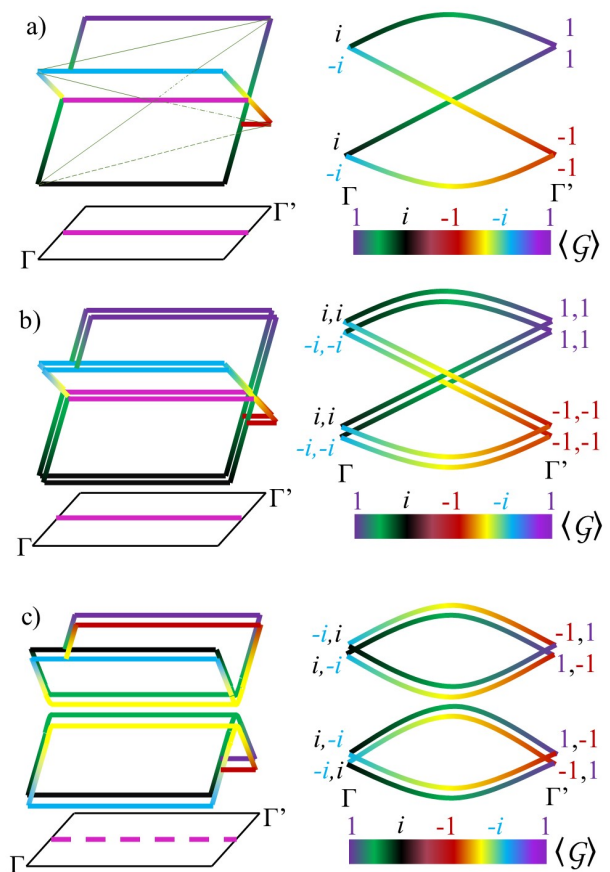


FIG. 1. Sketch of nodal lines and quasi-nodal lines on glide reflection symmetry planes. (a) The hourglass defined by the energy bands on any path between the TRIMs Γ and Γ' forces the existence of a nodal line on the symmetry plane. In the presence of inversion the energy bands degenerate and the two bands have the same \mathcal{G} eigenvalue (b) or eigenvalues of opposite sign (c). Whenever the degenerate bands have same \mathcal{G} eigenvalue, then the existence of a double nodal line is enforced (b). Whenever the degenerate bands have \mathcal{G} eigenvalues of opposite sign, the bands hybridize and the crossing is avoided (c). In the latter case, whenever the energy gap is small (~ 25 meV), we call the anticrossings *quasi-nodal lines*. In all three panels the colored bar parametrizes the \mathcal{G} eigenvalues of the energy bands. In panels b) and c) the bands are degenerate but for the sketch's clarity the bands have been separated.

operator \mathcal{G} shown in Eqn. (8). On these planes we may diagonalize Ψ as follows:

$$\mathcal{G}\Psi(\mathbf{k}) = \pm i e^{-i\mathbf{k}\cdot\mathbf{b}_{\mathbf{n}^\perp}} \Psi(\mathbf{k}). \quad (10)$$

Replacing Ψ in Eqn. (9) we obtain the \mathcal{G} eigenvalues for $(\mathbb{T}\mathcal{I})\Psi$ on the fixed planes:

$$\mathcal{G}((\mathbb{T}\mathcal{I})\Psi(\mathbf{k})) = \mp (e^{-i2\mathbf{k}\cdot\mathbf{b}_{\mathbf{n}^\perp}}) i e^{-i\mathbf{k}\cdot\mathbf{b}_{\mathbf{n}^\perp}} ((\mathbb{T}\mathcal{I})\Psi(\mathbf{k})). \quad (11)$$

We see that the \mathcal{G} -eigenvalues of both Ψ and its Kramer pair $(\mathbb{T}\mathcal{I})\Psi$ differ by the phase factor $-e^{-i2\mathbf{k}\cdot\mathbf{b}_{\mathbf{n}^\perp}}$. This

phase is always -1 except in the case that $\mathbf{b}_n \neq 0$, the unit normal vector \mathbf{n} is in the list of (4) and the fixed plane is $k_l = \pi$; in this case the phase factor is 1.

Therefore the pair of bands Ψ and $(\mathbb{T}\mathbb{Z})\Psi$ have always opposite sign \mathcal{G} eigenvalues, except on the case that $\mathbf{b}_n \neq 0$, \mathbf{n} is in (4) and the fixed plane is $k_l = \pi$. In this case we have that $2\mathbf{k} \cdot \mathbf{b}_n = \mathbf{k} \cdot \mathbf{n} = \pi$ and therefore the bands Ψ and it $(\mathbb{T}\mathbb{Z})\Psi$ have the same \mathcal{G} eigenvalue.

We may therefore infer that unless $\mathbf{b}_n \neq 0$, \mathbf{n} is in (4) and the fixed plane is $k_l = \pi$, the energy crossing between a pair of double bands along the fixed planes of \mathcal{G} is avoided due to hybridization. Each double band has both \mathcal{G} eigenvalues, therefore energy repulsion (hybridization) occurs at all points where the double bands get closer in energy (see Fig. 1 (c) for a schematic diagram of this hybridization). This effect is also called *anticrossing of bands* since the energy gap thus formed between the bands may be very small and therefore a nodal line might be computational and experimentally detected. The gap thus formed depends on the intensity of the SOC and therefore it may be small. Whenever the energy gap of these anticrossings is small the physical effects are relevant and therefore we may call these anticrossings with the name *quasi-nodal line*. The rhombohedral trifluorides and trioxides fall into this category of materials.

Whenever $\mathbf{b}_n \neq 0$, \mathbf{n} is in (4) and the fixed plane is $k_l = \pi$, the \mathcal{G} eigenvalues of the Kramer degenerate pairs are equal. Therefore if the reflection symmetry \mathcal{G} predicted nodal lines as presented before, inclusion of the inversion operator keeps the nodal lines. Now they are nodal lines of double degenerate Kramer's pairs. Originally the nodal lines were protected by the hourglass argument that produces \mathcal{G} , and since the Kramer's pairs have the same \mathcal{G} eigenvalues, the hourglasses are now double degenerate and also protected (see Fig. 1 (b) for a schematic diagram of these double nodal lines).

Let us see what does the inclusion of the inversion symmetry do on the examples we presented on the previous section. For the reflections considered in a) and c), namely $\mathcal{G}(x, y, z) = (-x, y, z + \frac{1}{2})$ and $\mathcal{G}(x, y, z) = (y + \frac{1}{2}, x + \frac{1}{2}, z + \frac{1}{2})$ respectively, the absence of translation on the normal direction implies that the Kramer pairs of energy bands along the fixed planes have opposite \mathcal{G} eigenvalues. Therefore the energy crossings induced by the operator \mathcal{G} hybridize and we obtain nodal line anticrossings as the ones presented in Fig. 1 (c). The energy gap on these anticrossings depends on the intensity of the SOC, hence if the energy gap is small, these anticrossing may well behave like nodal lines (quasi-nodal lines). Nevertheless, they will not be topologically protected.

For the glide reflection considered in b) with $\mathcal{G}(x, y, z) = (-x + \frac{1}{2}, y, z + \frac{1}{2})$ we will have a nodal line anticrossings on the plane $k_x = 0$ like the one in Fig. 1 (c), meanwhile the double nodal lines appear on the plane $k_x = \pi$ as presented in Fig. 1 (b). On $k_x = 0$

the Kramer pair of energy bands possesses opposite \mathcal{G} eigenvalues, meanwhile on $k_x = \pi$ the eigenvalues are the same.

Quasi-nodal lines

We have seen in the previous sections how nodal lines appear and are topologically protected whenever there is a glide reflection symmetry and time reversal symmetry on the system. These nodal lines possess different properties in the presence of the inversion symmetry. The composition of the inversion with time reversal induces Kramer's degeneracy on the energy bands localized on the fixed planes of the glide reflection and depending on the type of glide reflection, the Kramer's pairs may have equal eigenvalues for the glide reflection operator or eigenvalues with opposite sign. In the former case, the double nodal lines that appear are topologically protected and they are also known as *Dirac nodal lines* [27]; in the latter case the bands hybridize and the band crossing is avoided.

The existence of protected nodal lines and double nodal lines close to the Fermi level induce exotic spin and electronic transport properties [39] on the material, among them resonant spin-flipped reflection [44] and anomalously Hall currents [45]. Therefore the existence of protected nodal lines has been extensively studied in the last years [26, 42]. On the other hand, nodal lines that hybridize due to the presence of the inversion symmetry have seldomly been studied [24]. The energy gap that appears due to the hybridization makes them of less interest. Nevertheless, whenever the gap that is opened due to hybridization is small, interesting electronic properties are induced on the material.

We have therefore coined the name of *quasi-nodal lines* for the lines on fixed \mathcal{G} planes that exist whenever there is a hybridization of nodal lines and whose energy gap is very small (comparable to room temperature ~ 25 meV). It could be argued that since these quasi-nodal lines are not topologically protected, their existence may not have any implication on the electronic properties of the materials. We would like to argue otherwise: since the energy gap opened due to hybridization is very small, the electronic properties detected are similar to the ones observed on nodal lines. Furthermore, if the quasi-nodal lines are close to the Fermi level, interesting phenomena on charge and spin transport are observed such as large anomalous and Nernst Hall effect, spin Hall effect, among others [38, 39, 46].

Rhombohedral materials crystallizing on symmetry groups # 161 and #167 and ferromagnetic groups #161.71 and #167.107 show the presence of quasi-nodal lines on their electronic structure. This is the content of the next section.

QUASI-NODAL LINES ON RHOMBOHEDRAL MATERIALS

Quasi-nodal lines are present on rhombohedral materials crystallizing on the symmetry groups #161 and #167 and on their ferromagnetic phases #161.71 and #167.107. Among the many materials crystallizing on these symmetry groups, the rhombohedral trifluorides and trioxides make a pair of interesting families of compounds to study. In both families there are compounds crystallizing in all four symmetry groups. In Table I we have summarized the properties of the symmetry groups and the materials with quasi-nodal lines on glide reflection planes.

The crystal symmetries that generate these four groups are

$$\mathcal{C}(x, y, z) = (y, z, x) \quad (12)$$

$$\mathcal{I}(x, y, z) = (-x, -y, -z) \quad (13)$$

$$\mathcal{G}(x, y, z) = (y + \frac{1}{2}, x + \frac{1}{2}, z + \frac{1}{2}) \quad (14)$$

$$\mathcal{R}(x, y, z) = (-y + \frac{1}{2}, -x + \frac{1}{2}, -z + \frac{1}{2}) \quad (15)$$

with \mathcal{C} a 3-fold rotation, \mathcal{I} inversion, \mathcal{G} a glide reflection and $\mathcal{R} = \mathcal{G}\mathcal{I}$. In momentum coordinates we have

$$\mathcal{R}(k_x, k_y, k_z) = (k_y, k_x, k_z) \quad (16)$$

$$\mathcal{G}(k_x, k_y, k_z) = (-k_y, -k_x, -k_z), \quad (17)$$

and the non-trivial relations (including SOC) among the generators are the following:

$$\mathcal{I}^2 = 1, \quad \mathcal{C}^3 = -1, \quad \mathcal{R}^2 = -1, \quad \mathcal{C}\mathcal{G} = \mathcal{G}\mathcal{C}^{-1} \quad (18)$$

$$\mathcal{C}(\mathbb{T}\mathcal{G}) = (\mathbb{T}\mathcal{G})\mathcal{C}^{-1} \quad (19)$$

$$\mathcal{G}^2 = -e^{-i\pi(k_x+k_y+k_z)} \quad (20)$$

$$(\mathbb{T}\mathcal{G})^2 = e^{-i\pi(k_x+k_y+k_z)} \quad (21)$$

$$\mathcal{R}\mathcal{I} = e^{i\pi(k_x+k_y+k_z)}\mathcal{I}\mathcal{R}, \quad (22)$$

$$\mathcal{G}\mathcal{I} = e^{-i\pi(k_x+k_y+k_z)}\mathcal{I}\mathcal{G}, \quad (23)$$

$$(\mathbb{T}\mathcal{G})\mathcal{I} = e^{-i\pi(k_x+k_y+k_z)}\mathcal{I}(\mathbb{T}\mathcal{G}). \quad (24)$$

Here we have $\mathbf{b}_{\mathbf{n}^\perp} = (\frac{1}{2}, \frac{1}{2}, \frac{1}{2})$, $\mathbf{b}_{\mathbf{n}} = (1, -1, 0)$ and the \mathcal{G} fixed planes are $k_x = k_y$, $k_y = k_z$ and $k_z = k_x$. The quasi-nodal lines appear on the planes fixed by \mathcal{G} and for all the four symmetry groups they have a multiplicity of 6 on the whole Brillouin zone. This is shown in Table I.

Due to the presence of the composition of inversion with time reversal on the materials with SG #167, the quasi-nodal lines appearing are Dirac quasi-nodal lines or double quasi-nodal lines. Whenever inversion is broken, as in the materials with SG #161, the Dirac quasi-nodal lines unfold in a pair of quasi-nodal lines and a pair of accidental nodal lines. In Fig. 2 a schematic diagram of each of the quasi-nodal lines on the four symmetry groups has been presented.

In the ferromagnetic rhombohedral trifluorides LiCuF_3 and PdF_3 (see Fig. 3) that we present in the next section,

Rhombohedral crystals with quasi-nodal lines				
	No Magnetic		Ferromagnetic	
SG #	167	161	167.107	161.71
Generators	$\mathcal{G}, \mathcal{I}, \mathbb{T}, \mathcal{C}$	$\mathcal{G}, \mathbb{T}, \mathcal{C}$	$\mathbb{T}\mathcal{G}, \mathcal{I}, \mathcal{C}$	$\mathbb{T}\mathcal{G}, \mathcal{C}$
Symmetries	24	12	12	6
Fixing planes	$\mathbb{T}\mathcal{I}, \mathcal{G}$	\mathcal{G}	$\mathbb{T}\mathbb{T}\mathcal{G}$	
Multiplicity of quasi-nodal line	6	6	6	6
Materials	IrF_3 InF_3 RhF_3 GaF_3 AlF_3 ScF_3	LaAgO_3 LaCuO_3 NaCdF_3 CaTiF_3 CsPbF_3	$\text{PdF}_3, \text{MnF}_3$ $\text{MnBO}_3, \text{NiF}_3$ $\text{LaMnO}_3, \text{VF}_3$ $\text{TiBO}_3, \text{RuF}_3$ $\text{LaNiO}_3, \text{MoF}_3$ $\text{CoF}_3, \text{RuF}_3$ $\text{FeF}_3, \text{CrF}_3$	LiCuF_3 LiVF_3

TABLE I. Rhombohedral crystals with quasi-nodal lines on the planes fixed by the glide reflection \mathcal{G} . The highlighted materials in red have nodal lines crossing the Fermi level. The group with the most symmetries is #167, which includes the 3-fold rotation \mathcal{C} , inversion \mathcal{I} , time reversal \mathbb{T} and the glide reflection \mathcal{G} ; whenever the inversion symmetry is broken we obtain the group #161. In the presence of magnetization along the axis of rotation of the 3-fold symmetry \mathcal{C} , time reversal \mathbb{T} is broken together with the glide reflection \mathcal{G} . The symmetry that is kept is the composition $\mathbb{T}\mathcal{G}$ thus defining the magnetic symmetry groups #167.107 in the presence of inversion, and #161.71 whenever the inversion is broken. The quasi-nodal lines appear on the planes fixed by \mathcal{G} ; their multiplicity is calculated as the number of total symmetries divided by the number of symmetries that fix the planes. In all four cases the multiplicity is 6.

the presence of the quasi-nodal lines has been observed. The valence and conduction bands restricted to the \mathcal{G} fixed plane can be seen in Fig 4 (a) and (a'), the quasi-nodal lines on the \mathcal{G} plane in Fig. 4 (c) and (c'), the graph of the nodal line versus the energy in Fig. 4 (f) and (f'), the hybridization of the energy bands on the anticrossings in Fig. 2 (c), 4 (d) and (d'), and the six-fold multiplicity of the quasi-nodal lines on the whole Brillouin zone in Fig. 4 (e) and (e').

The energy gaps along the quasi-nodal lines presented in Fig. 4 (e) and (e') are less than 0.6 meV in the case of LiCuF_3 and less of 3.0 meV in the case of PdF_3 . In both cases the quasi-nodal lines include Weyl points lying on the line Γ -T is fixed by the \mathcal{C} rotation. These Weyl points lie close to the point T and their existence can be deduced from the fact that the \mathcal{C} eigenvalues are different on the bands close to the Fermi level. Since the \mathcal{C} eigenvalues are different, the hybridization cannot be carried out and the crossing is topologically protected. These energy crossings along the symmetry line Γ -T close to the point T can be observed at the right hand side of all four panels in Fig. 3. Here the colors on the energy bands represent different \mathcal{C} eigenvalues. The fact that

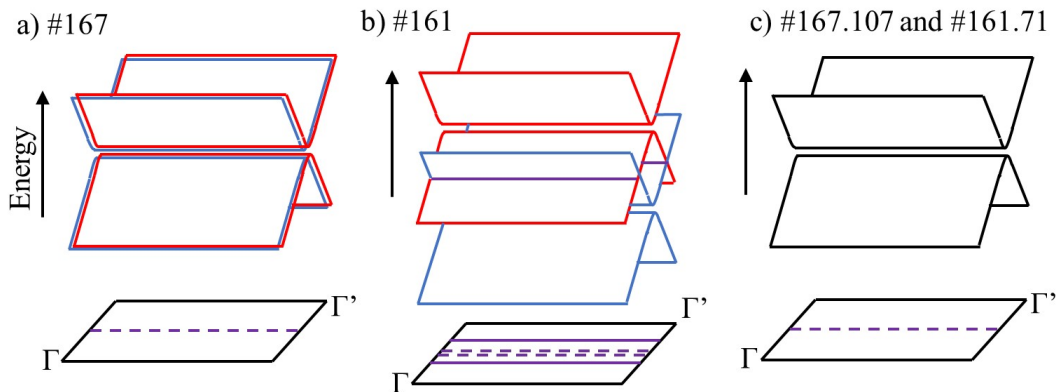


FIG. 2. Sketch of quasi-nodal lines on the four symmetry groups 167, 161, 167.107 and 161.71. (a) On the SG #167 the bands are degenerate and the eigenvalues of the operator \mathcal{G} have opposite sign which permits the bands to hybridize. (b) On the SG #161 the inversion symmetry is broken and the degenerate bands unfold. The bands with same color hybridize and the bands with opposite color intersect. Here we observe a pair of accidental nodal lines and a pair of quasi-nodal lines. In these two cases the red and blue bands have opposite \mathcal{G} eigenvalue. (c) On the magnetic SG # 167.107 and 161.71 the glide reflection \mathcal{G} symmetry is broken and therefore there is no restriction on the bands for their hybridization. In all four symmetry groups the quasi-nodal lines appear on the planes fixed by the glide reflection \mathcal{G} . These quasi-nodal lines have been detected on the non-magnetic and ferromagnetic rhombohedral trifluorides presented in Fig. 3.

the quasi-nodal lines include Weyl points implies that the bandgap energy along the quasi-nodal lines remains small. The existence of the Weyl points along the line Γ -T protects the quasi-nodal lines from being completely gapped.

Let us finish this section with an analysis of the corepresentations that appear on the points invariant by the inversion operator, i.e. $\Gamma(0, 0, 0)$, $L(0, 0, \pi)$, $F(0, \pi, \pi)$ and $T(\pi, \pi, \pi)$, and on the lines fixed by \mathcal{C} and $\mathbb{T}\mathcal{G}$.

The operator $\mathbb{T}\mathcal{G}$ has for fixed points the lines $k_x + k_y = 0$ on the planes $k_z = 0$ and $k_z = \pi$. By Eqn. (21) we see that $(\mathbb{T}\mathcal{G}) = 1$ on Γ and F and $(\mathbb{T}\mathcal{G}) = -1$ on L and T . The $k_x = k_y = k_z$ axis is fixed by the rotation operator \mathcal{C} and the eigenvalues of \mathcal{C} are $e^{\frac{il\pi}{3}}$ with $l = 1, 3, 5$. From the commutation relations presented in Eqn. (19) and (24) we deduce that on the points Γ and F the antiunitary operator $\mathbb{T}\mathcal{G}$ behaves like the complex conjugation operator \mathbb{K} , the inversion operator like multiplication by ± 1 , and on Γ , the operator \mathcal{C} is multiplication by $e^{\frac{il\pi}{3}}$ with $l = 1, 3, 5$. Hence on Γ and F the corepresentations are one-dimensional.

On T and L Eqn. (24) implies that $\mathbb{T}\mathcal{G}$ changes the sign of the \mathcal{I} eigenvalue and therefore the corepresentations are two-dimensional with the following matrix representation:

$$\mathcal{I} = \begin{pmatrix} +1 & 0 \\ 0 & -1 \end{pmatrix}, \quad \mathbb{T}\mathcal{G} = \begin{pmatrix} 0 & 1 \\ -1 & 0 \end{pmatrix} \mathbb{K}. \quad (25)$$

On T , because of Eqn. (19), the \mathcal{C} eigenvalues are repeated and its matrix representation is:

$$\mathcal{C} = \begin{pmatrix} e^{\frac{il\pi}{3}} & 0 \\ 0 & e^{\frac{il\pi}{3}} \end{pmatrix}. \quad (26)$$

On the right hand side of all four panels of Fig. 3 it can be observed that the energy bands with same \mathcal{C} eigenvalue join at T , thus agreeing with the previous matrix description, and that the energy crossings close to T with different \mathcal{C} eigenvalues define Weyl points [43]

Let us finally note that whenever we have the presence of time reversal and inversion, all bands are degenerate and the corepresentations defined above will appear with their Kramer's dual. On T and L points for the symmetry group #167 the energy bands have degeneracy four.

MATERIALS REALIZATION

Rhombohedral crystals are structures that fit into rhombohedral Bravais lattices with space groups #146, 148, 155, 160, 161, 166, or 167. Materials with these crystal lattices can present a layered structure with a hexagonal order within each layer, which is common in topological insulators as Bi_2Te_3 , Bi_2Se_3 and Sb_2Te_3 [47]. A broad kind of insulators and semiconductor materials as XF_3 -type, ABF_3 -type, ABO_3 -type, and $\text{AB}(\text{PO}_4)_3$ -type, crystallize in these rhombohedral phases with spaces groups #161 (R3c) and #167 (R3c). In particular, IrF_3 presents the most stable phase in the space group #167 with an indirect energy gap of 0.9 eV and an electronic band structure as it is shown in Fig. 3(a). The first conduction bands have a particular shape which is common in other materials with space groups #167 and #161. This electronic band structure presents two close bands in the L - T high symmetry line of the Brillouin zone, see Fig. 3(e), and depending on the material, the Fermi level can cross these close bands generating unique electronic and spin transport

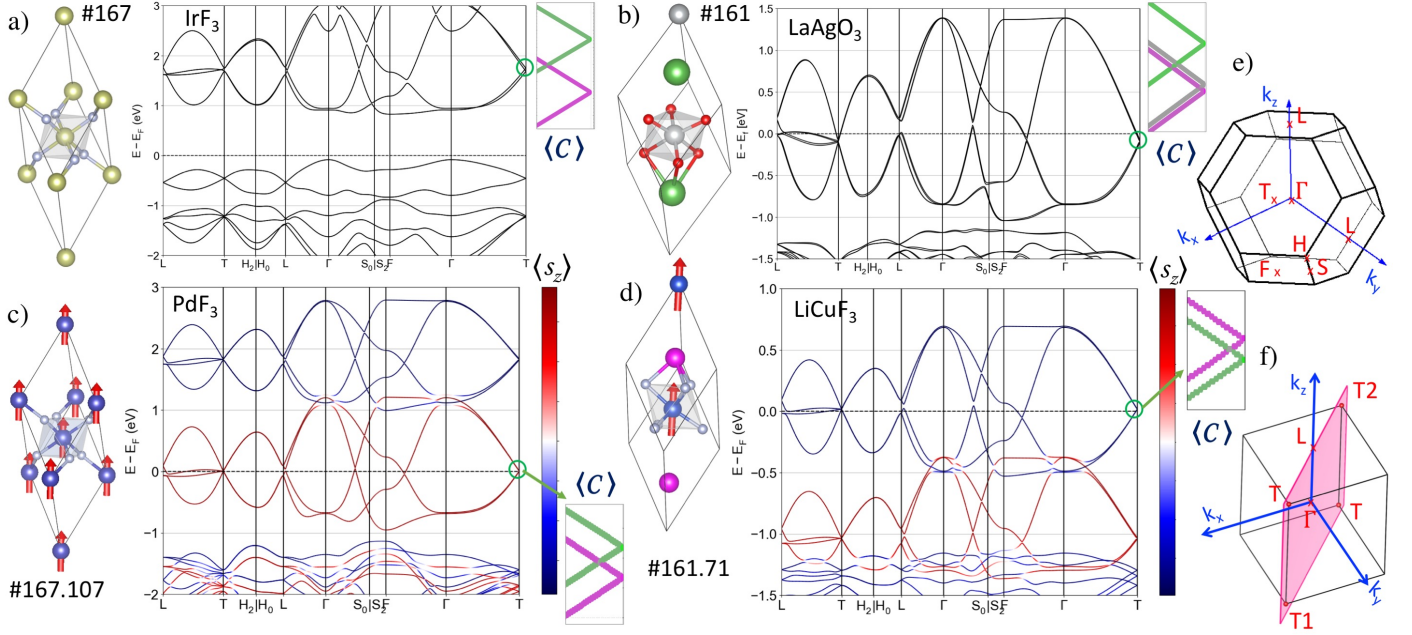


FIG. 3. Rhombohedral crystal structure and electronic band structure calculated for (a) IrF_3 (space group #167), (b) LaAgO_3 (space group #161), (c) PdF_3 (magnetic space group #167.107) and (d) LiCuF_3 (magnetic space group #161.71). Eigenvalues of the rotation $\langle C \rangle$ and the spin- z $\langle S_z \rangle$ operators projected on the electronic bands are shown. The zoom-in band structures near to the T point show the band crossings along the symmetry line Γ -T. (e) Brillouin zone of the rhombohedral structure with the labels of the high-symmetry points. (f) $(1\bar{1}0)$ plane on the reciprocal space of the rhombohedral structure.

properties. This is the case of the trifluoride LaAgF_3 , which crystallizes in the space group #161 as it is shown in Fig. 3(b). The material LaAgF_3 has two LaAgF_3 molecules per unit cell and every molecule has five atoms. In this case, due to the loss of the inversion symmetry with respect to the space group #167, the band structure presents unfolding.

On the other hand, it was recently discovered that magnetic topological insulators may prefer the rhombohedral phases as is the case of the material MnBi_2Te_4 [48]. Among the materials that can crystallize in the magnetic rhombohedral-type structure we may find the conductive transition-metal (TM) fluorides and oxides such as MnF_3 , CoF_3 , PdF_3 , FeF_3 , LiCuF_3 , MnBO_3 , LaMnO_3 , TiBO_3 and LaNiO_3 (See Table I). For the case of XF_3 , the primitive unit cell contains two transition-metal atoms surrounded by six F atoms that form an octahedron as it is shown in Fig. 3(c) and (d). Recently, it was found that the TM atoms can exhibit a ferromagnetic order in the z direction as it is shown in Fig. 3(c), where the local magnetic moments are indicated by arrows. Fig. 3 also shows the band structure along high-symmetry lines including the spin-orbit coupling interaction. Similar behavior is observed for LiCuF_3 materials, which also present a ferromagnetic stable structure oriented parallel to the z axis, as it is shown in Fig. 3(d).

The projection of the z -spin component is also shown in the band structure for the ferromagnetic cases. It can be noted a conductor behavior for the up (down) spin orientation in PdF_3 (LiCuF_3), but as an insulator for the opposite orientation. Consequently, the spin band polarization of the conduction of electrons is 100%, and therefore the longitudinal and transverse currents will be full spin-polarized. For PdF_3 and LiCuF_3 is obtained an opposite spin bandgap of around 2.14 eV and 4.10 eV, respectively. These results are in agreement with previous theoretical data [49–51]. It is worth remarking that the spin-polarized band structure at the Fermi level shows a similar shape as in the nonmagnetic case. In these cases, the Fermi level crosses the nearby bands in the L-T path, which generates band energies and bandgap contours at the plane $k_x = k_y$ as is shown in Fig. 4(a) and (a'), and Fig. 4(c) and (c'). It is also observed a band crossing between valence and conduction bands close to the T point. This special feature of the band structure can induce a large anomalous Hall conductivity (AHC) and spin Hall conductivity (SHC) at the Fermi level for the ferromagnetic and non-magnetic cases, respectively.

In the presence of SOC, the band structure and the symmetry group of the materials depend on the direction of the total magnetization. In the PdF_3 and LiCuF_3 cases, the lowest energy was found for the magnetization in the z direction. For the XF_3 case with $\mathbf{m} \parallel z$, the

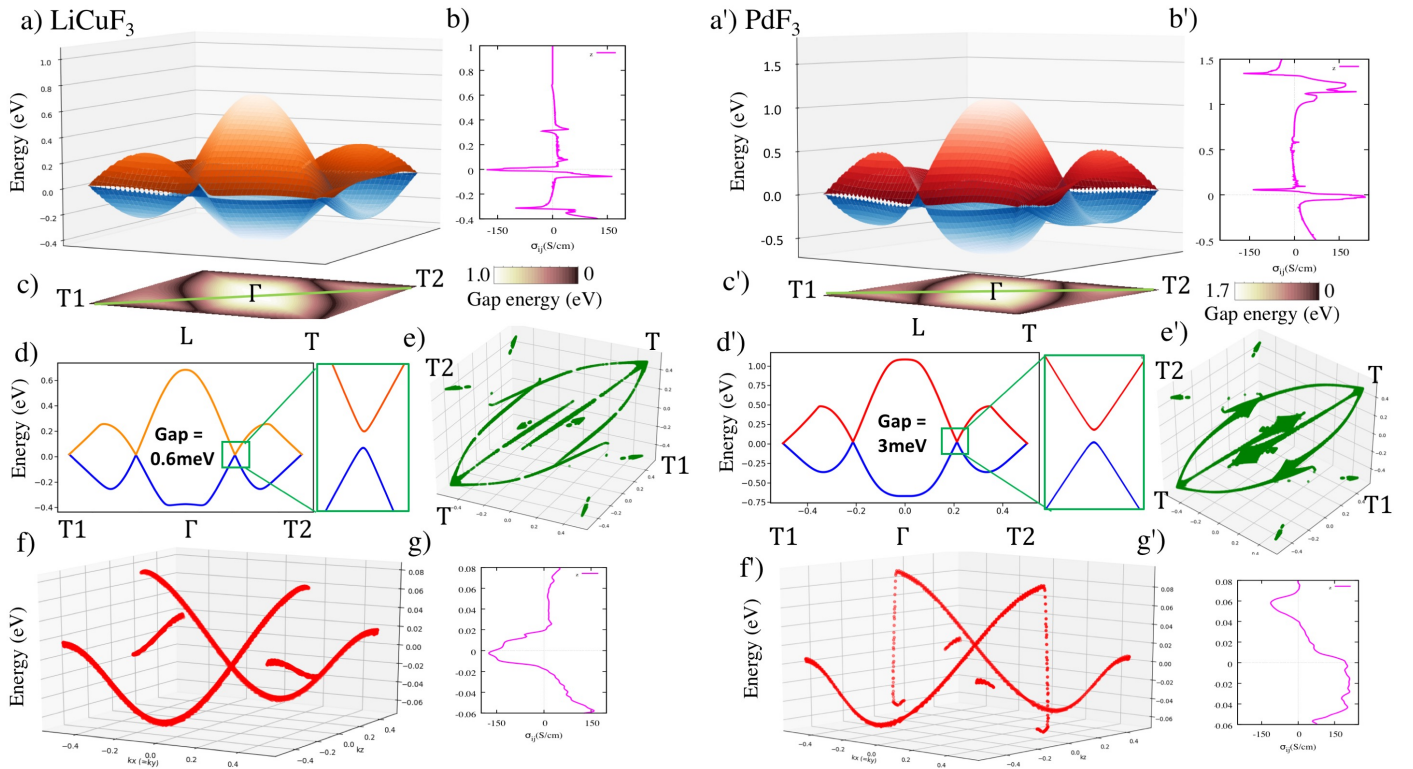


FIG. 4. Quasi-nodal lines and Anomalous Hall conductivity for the rhombohedral trifluorides LiCuF_3 and PdF_3 . (a) and (a'), energy of the valence and conduction bands restricted to the fixed \mathcal{G} plane $k_x = k_y$, (c) and (c') contour of the bandgap energy (difference between the conduction and the valence bands) and (f) and (f') quasi-nodal lines in the energy vs the plane $k_x (= k_y)$ and k_z space for the plane $(1\bar{1}0)$ shown in Fig. 3 (f). (d) and (d') calculated band structure for the T1- Γ -T2 k -path, and zoom around the anticrossing point showing the bandgap energy. (e) and (e'), structure of the 3D quasi-nodal lines in momentum space in which it is noted the C_3 symmetry around the T-T axis. (b), (b'), (g) and (g') anomalous Hall conductivity as a function of the Fermi level for LiCuF_3 in the magnetic space group #161.71 and for PdF_3 in the magnetic space group #167.107. The peaks of the AHC close to the Fermi level in diagrams (b) and (b') are located on the energy intervals where the quasi-nodal lines are defined. This fact can be appreciated in diagrams (f) and (g) for LiCuF_3 and (g') and (f') for PdF_3 where the location of the quasi-nodal lines on the energy level is compared to the AHC on the same energy.

#167 systems present the 167.107 magnetic space group with symmetries generated by \mathcal{I}, \mathcal{C} and the anti-unitary symmetry \mathcal{TG} . In the ABF_3 case with $\mathbf{m} \parallel z$, the #161 systems present the 161.71 magnetic space group with symmetries generated by \mathcal{C} and the anti-unitary symmetry \mathcal{TG} .

In the cases of XF_3 and ABF_3 with magnetic space groups 167.107 and 161.71, the multiple symmetries prohibits the anomalous Hall effect (AHE) in x and y components. The only component which is not constrained is $b_z(\mathbf{k}) \neq 0$, so the AHE should be observed with $\sigma_{xy} \neq 0$ as it is shown in Fig. 4(b) and (b'). These graphs show the variation of AHC for PdF_3 and LiCuF_3 with respect to the position of the Fermi energy. It is worth noting that the peaks of the AHC around the Fermi energy for σ_{xy} are as high as 180 S/cm. As it was pointed out before, close to the Fermi energy we have a full spin-polarized charge current and therefore we can consider the z -spin component as a good quantum number [52]. So the Hall current

carriers are one spin-polarized electron and the SHC can be calculated from the AHC by a factor of $2\hbar/e$, i.e. $\sim 90(\hbar/e)(\text{S/cm})$. These results were corroborated with the direct calculation of the SHC tensor.

In addition, it is found that the main contribution to the AHC at the Fermi level is due to the existence of the quasi-nodal lines close to the Fermi level. The main contribution to the AHC at top and bottom values of the Fermi energy is the electronic states generated by the quasi-nodal lines as it is shown in Fig. 4(g) and (g'). In Fig. 4(f) and (f') it is shown the energy distribution of the quasi-nodal lines as a function of $k_x (= k_y)$ and k_z ; these energies match the strong signal of the AHC in the energy window. The reciprocal space distribution of the quasi-nodal lines is shown in Fig. 4(e) and (e'), which shows clearly the six-fold multiplicity as indicated in the Table I and C_3 rotation symmetry around the T-T k -path. This corresponds to the main axis of C_3 symmetry in real space that characterizes the rhombohedral lattice structures. Finally, it is noted

the anticrossing band gap between the energy bands in Fig. 4(d) and (d') along the quasi-nodal line on the $k_x(=k_y)$ and k_z plane for the LiCuF_3 (0.6 meV) and PdF_3 (3.0meV).

COMPUTATIONAL METHOD

We have carried out *ab-initio* calculations within the density-functional theory (DFT) framework to study the formation of quasi-nodal lines in magnetic and nonmagnetic rhombohedral materials. Exchange and correlation effects were treated with generalized gradient approximation (GGA) [53], as implemented in the vienna *ab-initio* simulation package (VASP) [54]. The GGA+U method were employed for the PdF_3 material as presented in a recent report [50]. Spin orbit coupling (SOC) were included self-consistently in all the calculation. The electron wave function was expanded in plane waves up to a cut-off energy of 520 eV. A k -mesh of 0.02 ($2\pi/\text{\AA}$) k -space resolution was used to sample the Brillouin zone. DFT calculations of rhombohedral materials were performed using the refined lattice constants from the Materials project database [55]. In addition, we calculated the symmetry eigenvalues of the wavefunctions at the Brillouin zone using the irrep code [56].

In order to evaluate the electronic transport properties, we have used an effective tight-binding Hamiltonian constructed in the maximally localized Wannier basis [57] as a post-processing step of the DFT calculations. The intrinsic anomalous Hall conductivity (AHC) components were calculated by integrating the Berry curvature on a dense 230^3 k -mesh of the Brillouin zone [58]. Within this model, the AHC can be written as:

$$\sigma_{xy} = -\frac{e^2}{\hbar} \sum_n \int_{BZ} \frac{dk^3}{(2\pi)^3} f_n(k) \Omega_n^z(k) \quad (27)$$

Where $f_n(k)$ is the Fermi-Dirac distribution and the Berry curvature $\Omega_n^z(k)$ for the n th band can be calculated using the Kubo formula:

$$\Omega_n^z(k) = -2\hbar^2 \text{Im} \sum_{m \neq n} \frac{\langle n, k | \hat{v}_x | m, k \rangle \langle m, k | \hat{v}_y | n, k \rangle}{(\epsilon_{n,k} - \epsilon_{m,k})^2} \quad (28)$$

Where $|n, k\rangle$ are the Bloch functions of a single band n , k is the Bloch wave vector, $\epsilon_{n,k}$ is the band energy and \hat{v}_i is the velocity operator in the i direction.

DISCUSSION AND CONCLUSIONS

In this work we have put forward the concept of quasi-nodal lines. These are lines on the reciprocal space where the energy gap is very small. They appear due to the

hybridization of the nodal lines that glide reflection symmetries induce. The hybridization may be due to the inclusion of inversion symmetry, or due to magnetization which breaks the glide reflection symmetry. In both cases, if the gap generated by the hybridization is small, the quasi-nodal lines are present. In the family of rhombohedral trifluorides and trioxides, both ferromagnetic and non-magnetic, we have shown the existence of these quasi-nodal lines. Whenever the quasi-nodal lines are close to the Fermi level, interesting electronic transport properties are induced. This is the case of the ferromagnetic phase of PdF_3 and of LiCuF_3 where the presence of the quasi-nodal line on the Fermi level induces a large signal in the anomalous Hall conductance.

Quasi-nodal lines are not topologically protected. By this we mean that the energy gap could be adiabatically enlarged. Nevertheless, in practice the energy gap depends on the material structure and on the intensity of the SOC. Herein, by using *ab-initio* calculations, we have shown that the energy gap remains small for the materials mentioned above and therefore they could be detected experimentally. For the ferromagnetic phases, we have demonstrated a direct correspondence between the AHE (or SHE) signal and the existence of the quasi-nodal lines.

It is interesting to determine other families of materials on which quasi-nodal lines are also present. These families of materials may not crystallize with symmetry groups on which the nodal lines deem to exist, ie. the symmetry groups may not be on the list of symmetry groups with nodal lines. Nevertheless, the presence of quasi-nodal lines induce interesting electronic transport properties and therefore it is worth their future experimental research.

Quasi-nodal lines in ferromagnetic phases are due to the hybridization of nodal lines because the glide reflection symmetry is broken. It is interesting to note that the combinatorial structure of the bands is similar to the one of the material prior to the magnetization. This would mean that the magnetization, even though it breaks symmetries, it still remembers some of the information of the non-magnetic group. The reconstruction of quasi-nodal lines from the ferromagnetic symmetries is not straightforward; while the knowledge of the non-magnetic symmetries permits to infer the possible existence of these quasi-nodal lines.

ACKNOWLEDGEMENTS

The first author gratefully acknowledges the computing time granted on the supercomputer Mogon at Johannes Gutenberg University Mainz (hpc.uni-mainz.de). The second author thanks the German Service of Academic Exchange (DAAD) for its continuous support. The first and the third authors thank the continuous support

of the Alexander Von Humboldt Foundation, Germany.

* rhernandezj@uninorte.edu.co

† etuiran@uninorte.edu.co

‡ bjongbloed@uninorte.edu.co; uribe@mpim-bonn.mpg.de

- [1] D. Castelvechhi, *Nature* **547**, 272 (2017), ISSN 1476-4687, URL <https://doi.org/10.1038/547272a>.
- [2] M. Z. Hasan and C. L. Kane, *Rev. Mod. Phys.* **82**, 3045 (2010), URL <https://link.aps.org/doi/10.1103/RevModPhys.82.3045>.
- [3] A. Bansil, H. Lin, and T. Das, *Rev. Mod. Phys.* **88**, 021004 (2016), URL <https://link.aps.org/doi/10.1103/RevModPhys.88.021004>.
- [4] C.-K. Chiu and A. P. Schnyder, *Phys. Rev. B* **90**, 205136 (2014), URL <https://link.aps.org/doi/10.1103/PhysRevB.90.205136>.
- [5] A. A. Burkov, *Nature Materials* **15**, 1145 (2016), ISSN 1476-4660, URL <https://doi.org/10.1038/nmat4788>.
- [6] H. Gao, J. W. Venderbos, Y. Kim, and A. M. Rappe, *Annual Review of Materials Research* **49**, 153 (2019), <https://doi.org/10.1146/annurev-matsci-070218-010049>, URL <https://doi.org/10.1146/annurev-matsci-070218-010049>.
- [7] B. Yan and C. Felser, *Annual Review of Condensed Matter Physics* **8**, 337 (2017), <https://doi.org/10.1146/annurev-conmatphys-031016-025458>, URL <https://doi.org/10.1146/annurev-conmatphys-031016-025458>.
- [8] H. Weng, X. Dai, and Z. Fang, *J. Phys.: Condens. Matter* **28**, 303001 (2016), URL <https://link.aps.org/doi/10.1088/0953-8984/28/30/303001>.
- [9] N. P. Armitage, E. J. Mele, and A. Vishwanath, *Rev. Mod. Phys.* **90**, 015001 (2018), URL <https://link.aps.org/doi/10.1103/RevModPhys.90.015001>.
- [10] C. Gong, Y. Xie, Y. Chen, H.-S. Kim, and D. Vanderbilt, *Phys. Rev. Lett.* **120**, 106403 (2018), URL <https://link.aps.org/doi/10.1103/PhysRevLett.120.106403>.
- [11] T. Bzdusek, Q. Wu, A. Rüegg, M. Sigrist, and A. A. Soluyanov, *Nature* **538**, 75 (2016), ISSN 1476-4687, URL <https://doi.org/10.1038/nature19099>.
- [12] S. V. Syzranov and B. Skinner, *Phys. Rev. B* **96**, 161105(R) (2017), URL <https://link.aps.org/doi/10.1103/PhysRevB.96.161105>.
- [13] J. Hu, Z. Tang, J. Liu, Y. Zhu, J. Wei, and Z. Mao, *Phys. Rev. B* **96**, 045127 (2017), URL <https://link.aps.org/doi/10.1103/PhysRevB.96.045127>.
- [14] C. Wang, W.-H. Xu, C.-Y. Zhu, J.-N. Chen, Y.-L. Zhou, M.-X. Deng, H.-J. Duan, and R.-Q. Wang, *Phys. Rev. B* **103**, 165104 (2021), URL <https://link.aps.org/doi/10.1103/PhysRevB.103.165104>.
- [15] A. A. Burkov, *Phys. Rev. B* **97**, 165104 (2018), URL <https://link.aps.org/doi/10.1103/PhysRevB.97.165104>.
- [16] A. Laha, S. Mardanya, B. Singh, H. Lin, A. Bansil, A. Agarwal, and Z. Hossain, *Phys. Rev. B* **102**, 035164 (2020), URL <https://link.aps.org/doi/10.1103/PhysRevB.102.035164>.
- [17] Y. Shao, A. N. Rudenko, J. Hu, Z. Sun, Y. Zhu, S. Moon, A. J. Millis, S. Yuan, A. I. Lichtenstein, D. Smirnov, et al., *Nature Physics* **16**, 636 (2020), ISSN 1745-2481, URL <https://doi.org/10.1038/s41567-020-0859-z>.
- [18] Y.-C. Chiu, K.-W. Chen, R. Schönemann, V. L. Quito, S. Sur, Q. Zhou, D. Graf, E. Kampert, T. Förster, K. Yang, et al., *Phys. Rev. B* **100**, 125112 (2019), URL <https://link.aps.org/doi/10.1103/PhysRevB.100.125112>.
- [19] C. Fang, Y. Chen, H.-Y. Kee, and L. Fu, *Phys. Rev. B* **92**, 081201(R) (2015), URL <https://link.aps.org/doi/10.1103/PhysRevB.92.081201>.
- [20] Z.-M. Yu, W. Wu, X.-L. Sheng, Y. X. Zhao, and S. A. Yang, *Phys. Rev. B* **99**, 121106(R) (2019), URL <https://link.aps.org/doi/10.1103/PhysRevB.99.121106>.
- [21] S. Kobayashi, Y. Yamakawa, A. Yamakage, T. Inohara, Y. Okamoto, and Y. Tanaka, *Phys. Rev. B* **95**, 245208 (2017), URL <https://link.aps.org/doi/10.1103/PhysRevB.95.245208>.
- [22] C.-K. Chiu, J. C. Y. Teo, A. P. Schnyder, and S. Ryu, *Rev. Mod. Phys.* **88**, 035005 (2016), URL <https://link.aps.org/doi/10.1103/RevModPhys.88.035005>.
- [23] W. Wu, Y. Liu, S. Li, C. Zhong, Z.-M. Yu, X.-L. Sheng, Y. X. Zhao, and S. A. Yang, *Phys. Rev. B* **97**, 115125 (2018), URL <https://link.aps.org/doi/10.1103/PhysRevB.97.115125>.
- [24] S.-Y. Yang, H. Yang, E. Derunova, S. S. P. Parkin, B. Yan, and M. N. Ali, *Advances in Physics: X* **3**, 1414631 (2018), <https://doi.org/10.1080/23746149.2017.1414631>, URL <https://doi.org/10.1080/23746149.2017.1414631>.
- [25] J. Zou, Z. He, and G. Xu, *npj Computational Materials* **5**, 96 (2019), ISSN 2057-3960, URL <https://doi.org/10.1038/s41524-019-0237-5>.
- [26] B. Q. Lv, T. Qian, and H. Ding, *Rev. Mod. Phys.* **93**, 025002 (2021), URL <https://link.aps.org/doi/10.1103/RevModPhys.93.025002>.
- [27] Y. Kim, B. J. Wieder, C. L. Kane, and A. M. Rappe, *Phys. Rev. Lett.* **115**, 036806 (2015), URL <https://link.aps.org/doi/10.1103/PhysRevLett.115.036806>.
- [28] R. Yu, H. Weng, Z. Fang, X. Dai, and X. Hu, *Phys. Rev. Lett.* **115**, 036807 (2015), URL <https://link.aps.org/doi/10.1103/PhysRevLett.115.036807>.
- [29] J. Hu, Z. Tang, J. Liu, X. Liu, Y. Zhu, D. Graf, K. Myhro, S. Tran, C. N. Lau, J. Wei, et al., *Phys. Rev. Lett.* **117**, 016602 (2016), URL <https://link.aps.org/doi/10.1103/PhysRevLett.117.016602>.
- [30] R. Li, H. Ma, X. Cheng, S. Wang, D. Li, Z. Zhang, Y. Li, and X.-Q. Chen, *Phys. Rev. Lett.* **117**, 096401 (2016), URL <https://link.aps.org/doi/10.1103/PhysRevLett.117.096401>.
- [31] B. Feng, R.-W. Zhang, Y. Feng, B. Fu, S. Wu, K. Miyamoto, S. He, L. Chen, K. Wu, K. Shimada, et al., *Phys. Rev. Lett.* **123**, 116401 (2019), URL <https://link.aps.org/doi/10.1103/PhysRevLett.123.116401>.
- [32] I. Belopolski, K. Manna, D. S. Sanchez, G. Chang, B. Ernst, J. Yin, S. S. Zhang, T. Cochran, N. Shumiya, H. Zheng, et al., *Science* **365**, 1278 (2019), ISSN 0036-8075, <https://science.sciencemag.org/content/365/6459/1278.full.pdf>, URL <https://science.sciencemag.org/content/365/6459/1278>.
- [33] R.-W. Zhang, D.-S. Ma, J.-M. Zhang, and Y. Yao, *Phys. Rev. B* **103**, 195115 (2021), URL <https://link.aps.org/doi/10.1103/PhysRevB.103.195115>.
- [34] T. Yang, Z. Cheng, X. Wang, and X.-L. Wang, *Journal of Advanced Research* **28**, 43 (2021), ISSN 2090-

- 1232, URL <https://www.sciencedirect.com/science/article/pii/S2090123220301259>.
- [35] I. Belopolski, K. Manna, D. S. Sanchez, G. Chang, B. Ernst, J. Yin, S. S. Zhang, T. Cochran, N. Shumiya, H. Zheng, et al., *Science* **365**, 1278 (2019), ISSN 0036-8075, <https://science.sciencemag.org/content/365/6459/1278.full.pdf>, URL <https://science.sciencemag.org/content/365/6459/1278>.
- [36] S. F. Weber, R. Chen, Q. Yan, and J. B. Neaton, *Phys. Rev. B* **96**, 235145 (2017), URL <https://link.aps.org/doi/10.1103/PhysRevB.96.235145>.
- [37] C. Mera Acosta, E. Ogoshi, A. Fazzio, G. M. Dalpian, and A. Zunger, *Matter* **3**, 145 (2020), ISSN 2590-2385, URL <https://www.sciencedirect.com/science/article/pii/S2590238520302393>.
- [38] S. N. Guin, Q. Xu, N. Kumar, H.-H. Kung, S. Dufresne, C. Le, P. Vir, M. Michiardi, T. Pedersen, S. Gorovikov, et al., *Advanced Materials* **33**, 2006301 (2021), <https://onlinelibrary.wiley.com/doi/pdf/10.1002/adma.202006301>, URL <https://onlinelibrary.wiley.com/doi/abs/10.1002/adma.202006301>.
- [39] Y. Zhou, F. Xiong, W. Chen, and J. An, *Phys. Rev. B* **101**, 075125 (2020), URL <https://link.aps.org/doi/10.1103/PhysRevB.101.075125>.
- [40] N. Nagaosa, J. Sinova, S. Onoda, A. H. MacDonald, and N. P. Ong, *Rev. Mod. Phys.* **82**, 1539 (2010), ISSN 0034-6861, URL <http://link.aps.org/doi/10.1103/RevModPhys.82.1539>.
- [41] J. Sinova, S. O. Valenzuela, J. Wunderlich, C. H. Back, and T. Jungwirth, *Rev. Mod. Phys.* **87**, 1213 (2015), ISSN 0034-6861, 1411.3249, URL <http://link.aps.org/doi/10.1103/RevModPhys.87.1213>.
- [42] Y.-H. Chan, B. Kilic, M. M. Hirschmann, C.-K. Chiu, L. M. Schoop, D. G. Joshi, and A. P. Schnyder, *Phys. Rev. Materials* **3**, 124204 (2019), URL <https://link.aps.org/doi/10.1103/PhysRevMaterials.3.124204>.
- [43] R. González-Hernández, E. Tuiran, and B. Uribe, *Phys. Rev. B* **103**, 235143 (2021), URL <https://link.aps.org/doi/10.1103/PhysRevB.103.235143>.
- [44] W. Chen, K. Luo, L. Li, and O. Zilberberg, *Phys. Rev. Lett.* **121**, 166802 (2018), URL <https://link.aps.org/doi/10.1103/PhysRevLett.121.166802>.
- [45] W. B. Rui, Y. X. Zhao, and A. P. Schnyder, *Phys. Rev. B* **97**, 161113(R) (2018), URL <https://link.aps.org/doi/10.1103/PhysRevB.97.161113>.
- [46] J. Noky, Q. Xu, C. Felser, and Y. Sun, *Phys. Rev. B* **99**, 165117 (2019), URL <https://link.aps.org/doi/10.1103/PhysRevB.99.165117>.
- [47] H. Zhang, C.-X. Liu, X.-L. Qi, X. Dai, Z. Fang, and S.-C. Zhang, *Nature Physics* **5**, 438 (2009), ISSN 1745-2481, URL <https://doi.org/10.1038/nphys1270>.
- [48] Y. Deng, Y. Yu, M. Z. Shi, Z. Guo, Z. Xu, J. Wang, X. H. Chen, and Y. Zhang, *Science* **367**, 895 (2020), ISSN 0036-8075, <https://science.sciencemag.org/content/367/6480/895.full.pdf>, URL <https://science.sciencemag.org/content/367/6480/895>.
- [49] Y. Jiao, F. Ma, C. Zhang, J. Bell, S. Sanvito, and A. Du, *Phys. Rev. Lett.* **119**, 016403 (2017), URL <https://link.aps.org/doi/10.1103/PhysRevLett.119.016403>.
- [50] R.-W. Zhang, Z. Zhang, C.-C. Liu, and Y. Yao, *Phys. Rev. Lett.* **124**, 016402 (2020), URL <https://link.aps.org/doi/10.1103/PhysRevLett.124.016402>.
- [51] X. Wang, R. Khenata, Y. Han, Z. Cheng, H. Khachai, A. Aliev, and T. Yang, *Journal of Alloys and Compounds* **804**, 554 (2019), ISSN 0925-8388, URL <https://www.sciencedirect.com/science/article/pii/S0925838819319991>.
- [52] Y. Jiao, F. Ma, C. Zhang, J. Bell, S. Sanvito, and A. Du, *New Journal of Physics* **15**, 033014 (2013), URL <https://iopscience.iop.org/article/10.1088/1367-2630/15/3/033014>.
- [53] J. P. Perdew, K. Burke, and M. Ernzerhof, *Phys. Rev. Lett.* **77**, 3865 (1996), ISSN 0031-9007, URL <http://link.aps.org/doi/10.1103/PhysRevLett.77.3865>.
- [54] G. Kresse and J. Furthmüller, *Phys. Rev. B* **54**, 11169 (1996), URL <https://link.aps.org/doi/10.1103/PhysRevB.54.11169>.
- [55] A. Jain, S. P. Ong, G. Hautier, W. Chen, W. D. Richards, S. Dacek, S. Cholia, D. Gunter, D. Skinner, G. Ceder, et al., *APL Materials* **1**, 011002 (2013).
- [56] M. Iraola, J. L. Mañes, B. Bradlyn, T. Neupert, M. G. Vergniory, and S. S. Tsirkin, *Irrep: symmetry eigenvalues and irreducible representations of ab initio band structures* (2020), 2009.01764.
- [57] A. A. Mostofi, J. R. Yates, G. Pizzi, Y.-S. Lee, I. Souza, D. Vanderbilt, and N. Marzari, *Computer Physics Communications* **185**, 2309 (2014), ISSN 0010-4655, URL <http://www.sciencedirect.com/science/article/pii/S001046551400157X>.
- [58] S. S. Tsirkin, *npj Computational Materials* **7**, 33 (2021), ISSN 2057-3960, URL <https://doi.org/10.1038/s41524-021-00498-5>.